ELSEVIER

Cement & Concrete Composites 24 (2002) 331–338

Cement & Concrete Composites

www.elsevier.com/locate/cemconcomp

Phases formed during hydration of tetracalcium aluminoferrite in 1.0M magnesium sulfate solutions

B.A. Clark, P.W. Brown *

Department of Materials Science and Engineering, The Pennsylvania State University, University Park, PA 16802, USA

Abstract

Phase formation during tetracalcium aluminoferrite (C_4AF) hydration in 1.0 M $MgSO_4$ solution was investigated by isothermal calorimetry at 50 °C, X-ray diffraction (XRD), and scanning electron microscopy (SEM) analyses. Hydration reactions initially produced gypsum. SEM observations indicated the gypsum, which formed initially, to consist of fine particles (< 5 μm); these increased in size and amount with hydration time. Complex phase assemblages including gypsum, ettringite, and monosulfate were present at intermediate times. Monosulfate was the final crystalline hydration product. No crystalline phases incorporating iron were observed regardless of hydration time. Two amorphous phases were observed by SEM. These were calcium/iron-rich and magnesium/aluminum/sulfur-rich gels. The magnesium/aluminum compounds observed were formed as interfaces between the anhydrous C_4AF and aluminosulfate compounds. © 2002 Published by Elsevier Science Ltd.

Keywords: Sulfate solutions; Hydration; Phase formation

1. Introduction

A number of investigations have examined intrusion of magnesium and/or sodium sulfate solutions into hydrated mortars or concretes [1–6]. The primary deterioration mechanisms observed in these studies included decalcification of the cement paste and loss of calcium hydroxide as ettringite and brucite are formed. Gollop and Taylor [2,3,7] concluded ettringite formation caused expansion and cracking.

Taylor [8,9] attributes any form of sulfate attack (regardless of sulfate source) to the formation of ettringite and/or gypsum. Taylor [9] also indicates that monosulfate inter-dispersed with calcium silicate hydrate (C–S–H) can convert to ettringite; Gollop and Taylor [7] observed the same phenomena during magnesium sulfate solution intrusion.

Taylor also summarized the state of knowledge of ferrite phase hydration [10,11]. Various studies have examined the effects of precursor particle size, ferrite composition and sulfate composition on the rate of hydration [12–14]. Fukuhara et al. [14] and Brown [15] suggested the existence of an iron-rich amorphous phase and found evidence for such. Brown [16] also showed that monosulfate is formed from ettringite more rapidly during C_4AF hydration than during that of C_3A with a comparable surface area.

Lea [17] attributed the deleterious effects of magnesium sulfate attack in field concrete to expansion and cracking caused by the formation of gypsum and brucite. The kinetics of ferrite hydration has been shown to change in the presence of alkali [18,19]. However, the kinetics of ferrite phase hydration in magnesium sulfate solutions appear not to have been systematically studied before the present series investigations [20,21].

Our recent studies examined the effects of temperature and magnesium sulfate ($MgSO_4$) solution concentration on the hydration of C_4AF and on the hydration products produced at temperatures between 25 and 80 °C [20,21]. The XRD examinations of ferrite reactivity indicate it increases with $MgSO_4$ concentration and hydration temperature, while forming relatively simple phase assemblages. Our SEM studies of the products formed at a single temperature (50 °C) and $MgSO_4$ concentration (1.0 M) indicate the formation of a complex phase assemblage and suggest that magnesium aids aluminum mobility, promoting AFm compound formation. The kinetics of hydration at 50 °C and in 1.0 M $MgSO_4$ are examined in

* Corresponding author.
E-mail address: etx@psu.edu (P.W. Brown).

0958-9465/02/$ - see front matter © 2002 Published by Elsevier Science Ltd.
PII: S0958-9465(01)00084-1

the present study. The present study describes the evolution of phase assemblages as characterized by isothermal calorimetry, SEM and XRD analyses.

2. Methods and materials

The C_4AF powder (3300 cm^2/g) used in our previous studies [20,21] was also used in this investigation. Isothermal calorimetry was performed using the experimental setup described by TenHuisen [22]. Approximately 1.00 g of C_4AF was hydrated in 3.0 ml of 1.0 M $MgSO_4$ solution. The C_4AF and syringe containing the solution were allowed to reach thermal equilibrium before mixing. After mixing and when no further heat evolution could be detected, the solids present were removed from the calorimeter, washed with acetone and allowed to air dry before XRD or SEM characterization. These solids were hand ground in an agate mortar and pestle to produce an approximate 325-mesh powder.

XRD analyses were carried out at a scanning rate of 2° per minute between 5° and 55° 2Θ, using a Scintag 3100 system powder diffraction unit.

A RJ Lee Instruments PSEM® equipped with a light element; Noran Instruments energy dispersive spectrometer (EDS) was used for SEM analysis. Backscattered electron (BSE) imaging was used to perform the analyses. Two sample preparation techniques were used for the analyses. In the first, the powder was embedded in a low viscosity epoxy resin. The resulting 3/4 in. disk was then polished with 400, 600, and 1000 diamond grit and finally hand-lapped with 3 and 1 μm diamond polishing compound. This procedure permitted cross-sections of individual particles in the powder to be produced. In the second preparation technique, the powder was deposited evenly across a polycarbonate filter using acetone. A section of the filter was then attached to a SEM mount and carbon coated.

3. Results

3.1. Calorimetry

Fig. 1 shows the rate of heat liberation (W/mol of Al_2O_3) during hydration of C_4AF in 1.0 M $MgSO_4$ solution at 50 °C. Four peaks are evident. These are an initial mixing peak, a second peak (after an induction period), and two overlapping major peaks. The events leading to an initial hydration peak are complete after 2 h and the onset of a second hydration peak is observed after an induction period of 3 h. Heat was produced by the hydration reaction for 25 h, with a total maximum heat output of approximately 190 kJ/mol Al_2O_3. Companion samples were hydrated for 10 min, 4.7, 6.5, 10.6 and 30 h to permit XRD and SEM analyses to establish the hydration reactions causing the events observed by calorimetry.

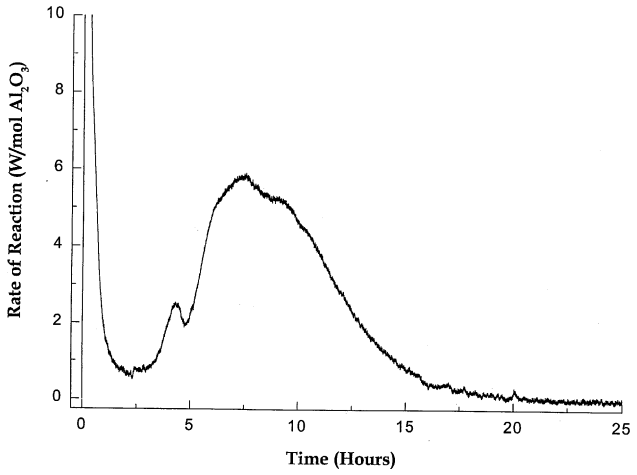

Fig. 1. Rate of heat evolved when C_4AF powder is hydrated in 1.0 M $MgSO_4$ solution.

3.2. X-ray diffraction analyses

Figs. 2 and 3 show the XRD patterns of solids obtained after various hydration times. These patterns indicate the presence of the following crystalline phases: the anhydrous ferrite phase (Ca_2AlFeO_5), monosulfate (AFm) ($Ca_4Al_2(OH)_{12} \cdot (SO_4) \cdot 6H_2O$), ettringite (AFt) ($[Ca_3Al(OH)_6 \cdot 12H_2O]_2(SO_4)_3 \cdot 2H_2O$), gypsum ($CaSO_4 \cdot 2H_2O$), calcium aluminum hemicarbonate hydrate ($4CaOAl_2O_3 \cdot 1/2CO_2 \cdot 12H_2O$: carbonate AFm), and a magnesium aluminum hydroxide hydrate ($Mg_4Al_2(OH)_{14} \cdot 3H_2O$). The amounts of these phases vary with the time of hydration. Residual ferrite was observed in each of the samples, except for that hy-

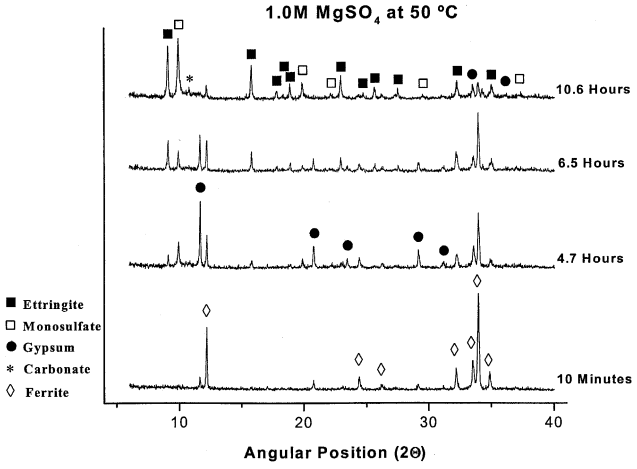

Fig. 2. XRD patterns obtained when C_4AF powder is hydrated for 10 min, 4.7, 6.5 and 10.6 h in 1.0 M $MgSO_4$ solution.

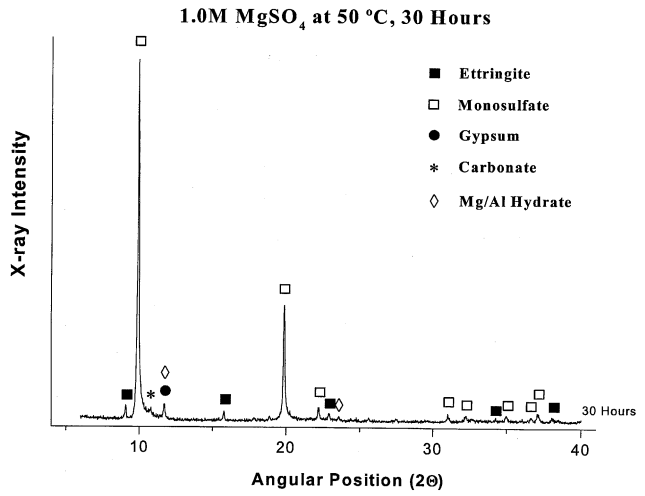

Fig. 3. XRD patterns obtained when C_4AF powder is hydrated for 30 h in 1.0 M $MgSO_4$ solution.

drated for 30 h. Gypsum was the initial hydration product. The amount of gypsum increased in samples hydrated for 10 min and 4.7 h and decreased thereafter. The proportions of monosulfate and ettringite varied with hydration time and indicate a complex interplay between the two phases. The phases observed by XRD in each of the samples are presented in Table 1. Calcium hydroxide, magnesium hydroxide and iron-containing crystalline phases were not observed.

3.3. Scanning electron microscopy analyses

Fig. 4 shows a BSE image of a cross-sectioned powder particle from the sample hydrated for 10 min. A particle comprised of two light but contrasting phases surrounded by the dark epoxy matrix is observed. The numbered points indicate the positions of EDS spot mode analyses, while Fig. 5 shows the EDS spectra obtained. All three spectra show compositions that contain aluminum, calcium and iron. Point #1 shows a spectrum of anhydrous C_4AF whereas the darker regions surrounding, points #2 and 3, show elevated aluminum contents.

Fig. 6 shows BSE images of particles deposited on to a polycarbonate filter surface obtained after 4.7 h of hydration. Five distinct particle types are observed and are labeled as gypsum, agglomerate or residual C_4AF.

Fig. 7 shows representative EDS spectra taken from the particles shown in Fig. 6. Points #1, 2, 5 and 6 showed compositions containing magnesium, aluminum, sulfur, calcium and iron. These points were all indicative of residual C_4AF and mixtures of other phases. Only calcium and sulfur are observed at points 3 and 4, indicating these particles are gypsum. The spectra from points #1 and 4 are presented in Fig. 7. The spectrum from point #1 is characteristic of anhydrous ferrite with AFm also present and is consistent with monosulfate formation from the ferrite phase and the Mg/S solution. Points #5 and 6 are also consistent with AFm formation, whereas the spectrum from point #2 is consistent with ettringite formation.

Fig. 8 shows a BSE image of particles obtained after C_4AF was hydrated for 6.5 h. Crystallites showing morphologies typical of gypsum or ettringite are present. Compared to the gypsum crystallite seen in Fig. 6, that in Fig. 8 appears to be partially consumed. The EDS spectra shown in Fig. 9 confirm the presence of gypsum and ettringite.

Fig. 10 shows a BSE image of a cross-sectioned polymineralic particle present after 10.6 h of hydration. Three distinct zones are evident in the image: (1) a nearly white zone containing an internal structure which is indicative of grain boundaries, (2) a light gray zone which surrounds the white zone and (3) a series of dark gray elongated structures which surround the lighter gray zone. Points #3, 6 and 7, shown in Fig. 11, illustrate the EDS spectra obtained from these zones. Point #1 is indicative of the C_4AF composition (see Fig. 5). Point #2 is similar to point #1, but indicates S to be present. The spectra obtained from points #2, 3, 4 and 5 are similar; the heights of the Ca, Al and S peaks are consistent with AFm, although the amounts of iron and magnesium vary. The morphology observed in the region around point #5 is that expected for AFm. The composition at point #6 is calcium and iron-rich with a small proportion of sulfur and aluminum present, consistent with a Ca/Fe-rich gel that was observed in a previous study [20]. The composition of point #7 is also similar to that of points #2, 3, 4, and 5 except that a Mg-containing phase is also present.

Table 1
Phases determined by XRD

Hydration time	Observed phases	Phases not detected
10 min	Mostly residual C_4AF, small amount gypsum	AFm, AFt, or Mg/Al hydrate
4.7 h	Less residual C_4AF, most gypsum, small amounts of AFt and AFm	Mg/Al hydrate
6.5 h	Less residual C_4AF, less gypsum, increased amounts of AFt and AFm	Mg/Al hydrate
10.6 h	Much less residual C_4AF, equal amounts of AFT and AFm	Gypsum, Mg/Al hydrate
30 h	Trace gypsum (?), Mg/Al hydrate, small amount AFt, most AFm	Residual C_4AF

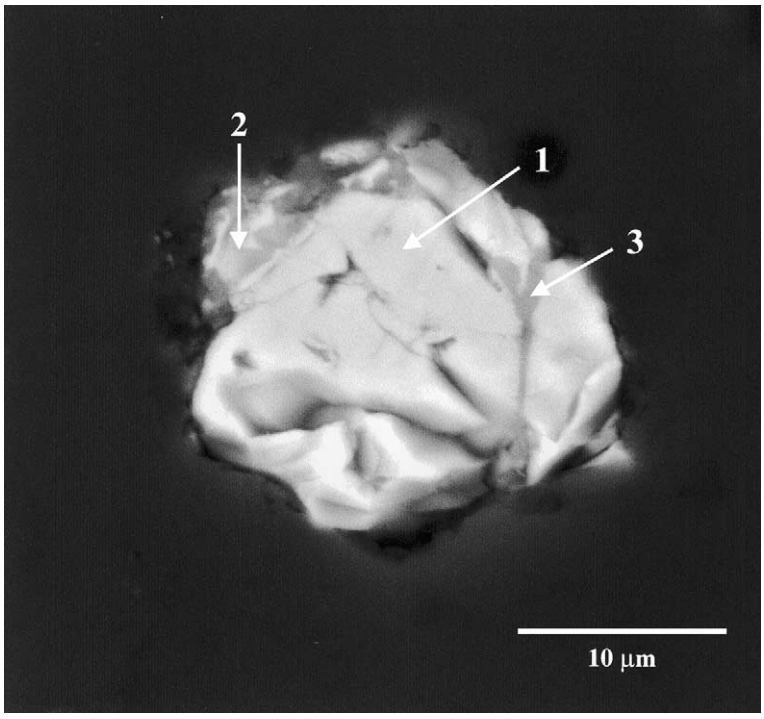

Fig. 4. BSE image of a cross-sectioned particle obtained when C_4AF powder is hydrated in 1.0 M $MgSO_4$ solution for 10 min.

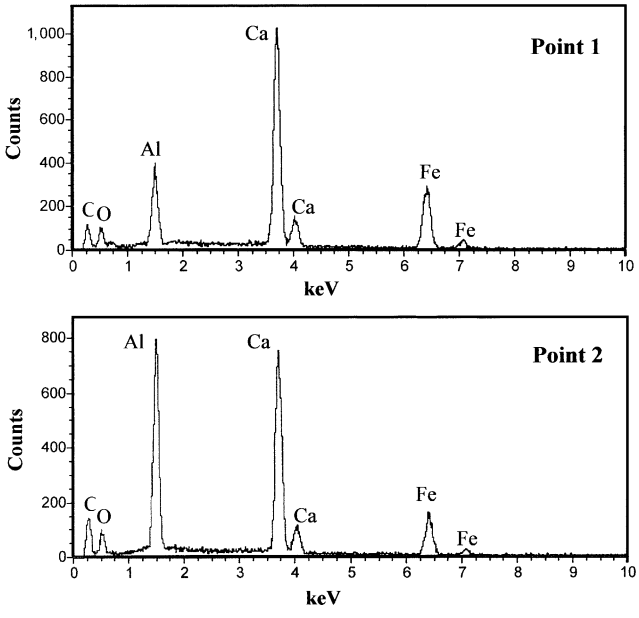

Fig. 5. EDS spectra obtained from points labeled in Fig. 4.

4. Discussion

4.1. Kinetics of phase evolution

The XRD and SEM data indicate minimal hydration before the induction period. XRD analysis indicated only a small amount of gypsum to have formed. The microstructures and EDS spectra shown in Figs. 4 and 5, exhibit no indication of hydration. Although the spectra indicate compositional variations within the ferrite phase and the formation of gypsum requires some ferrite phase hydration, none could be discerned by the SEM.

Only after the induction period, had significant gypsum formed. It is accompanied by the formation of an amorphous phase containing magnesium and aluminum. SEM indicates a portion of the gypsum to be comprised of < 5 μm crystallites, which eventually grow to dimensions of 10 μm by 30 μm. As calcium removal from the C_4AF is required for gypsum formation, a residual gel rich in aluminum and iron is also produced.

The XRD patterns of the samples hydrated for 4.7 and 6.5 h show the presence of small amounts of ettringite and monosulfate. The XRD patterns show the amount of gypsum to increase and then to decrease with hydration time, indicating it is being consumed in ettringite and monosulfate formation. Evidence for consumption is seen in the morphological differences between gypsum particles in Figs. 6 and 8.

After 10.6 h of hydration, the microstructure has changed substantially. XRD analysis indicates the complete consumption of gypsum and the presence of substantial amounts of ettringite and monosulfate. SEM analysis of polished cross-sections (Figs. 10 and 11) show structures indicating sulfate has reacted with the

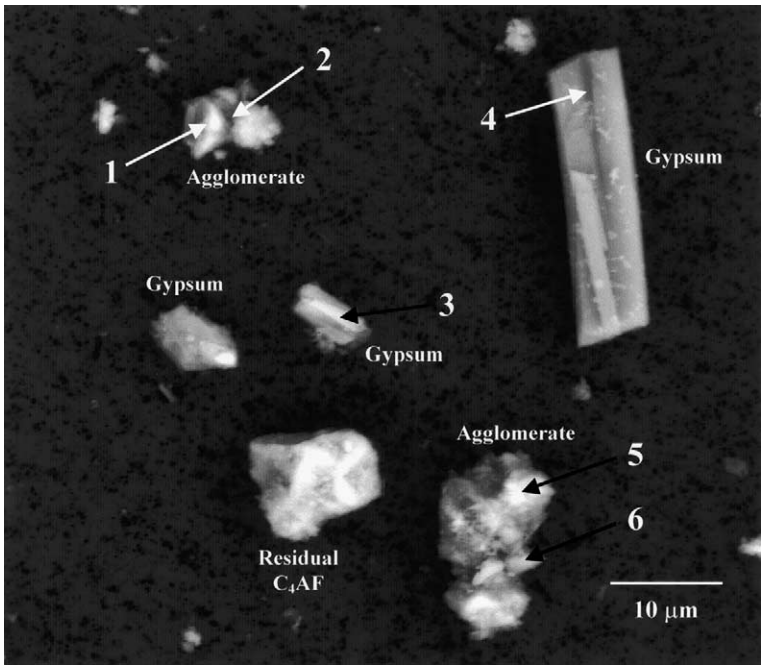

Fig. 6. BSE image of particulate obtained when C_4AF powder is hydrated in 1.0 M $MgSO_4$ solution for 4.7 h.

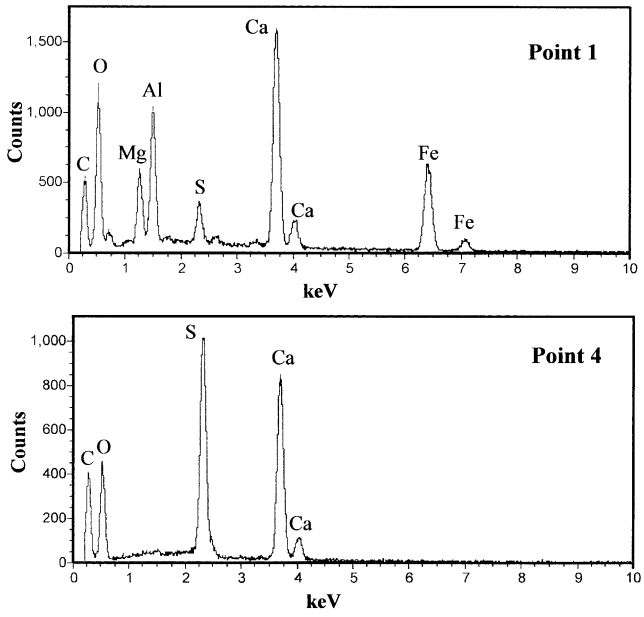

Fig. 7. EDS spectra obtained from points labeled in Fig. 6.

ferrite grains to form monosulfate. A rim of reaction products surrounds the residual ferrite particle (Fig. 10). An Al concentration gradient from the reaction rim toward the ferrite core and monosulfate formation indicates the leaching of Al from the ferrite phase. These processes also produce Fe-rich phases.

Comparison of samples hydrated at 6.5 and 10.6 h indicate that ettringite has formed and is converting to monosulfate after 6.5 h of hydration. As with gypsum, the amount of ettringite increases and then decreases with hydration time, indicating monosulfate is forming at the expense of ettringite. Based on these data, three mechanistic paths are therefore possible: (1) direct AFt formation followed by conversion to AFm, (2) direct AFm formation, conversion to AFt followed by conversion to AFm and (3) direct AFm formation from the ferrite/$MgSO_4$ interaction. Based on the relative amounts of gypsum, AFm and AFt observed with hydration time, the first mechanistic path is the most probable and is supported by the literature [12,16,23].

A prior SEM image of C_4AF hydrated in 1.0 M $MgSO_4$ solution [20] showed a morphology consistent with ettringite, while having a composition of monosulfate. This observation also supports the conclusion that hydration followed the first mechanistic path described above; ettringite formed initially followed by AFm conversion, while retaining the first polymorph structure.

Prior analysis [21] of the hydration of C_4AF in 1.0 M $MgSO_4$ solution, at an Al/SO_4 ratio insufficient to form AFt as a final product, indicated the overall reaction to be:

$$C_4AF + MgSO_4 \rightarrow AFm + \text{Fe-rich phases} + \text{Mg-rich phases} \quad (I)$$

The present XRD analyses show this reaction to occur in three stages. In stage 1 the initial hydration product is gypsum, along with magnesium and iron/aluminum gels. In stage 2 AFm and AFt form while gypsum is consumed. However, AFm appears prior to this

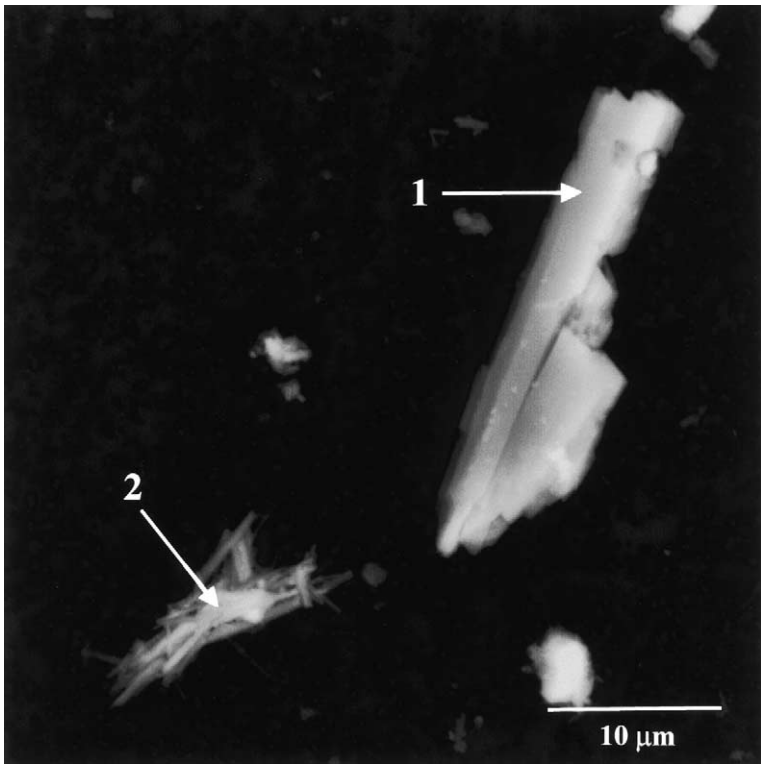

Fig. 8. BSE image of particulate obtained when C_4AF powder is hydrated in 1.0 M $MgSO_4$ solution for 6.5 h.

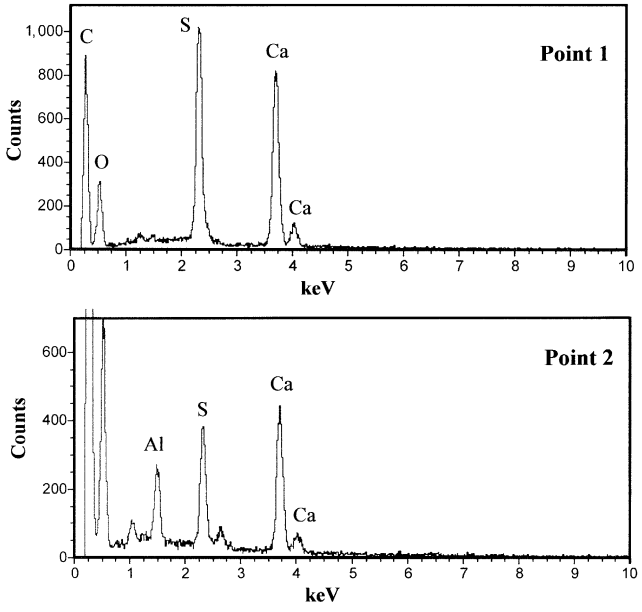

Fig. 9. EDS spectra obtained from points labeled in Fig. 8.

consumption of gypsum. In stage 3 hydration of residual C_4AF results in the consumption of AFt, resulting in AFm formation. This results in a final phase assemblage of AFm, Mg-containing phases and Fe-containing phases. Fig. 12 shows the relationship between these stages and the rate of heat evolution at 50 °C.

The present study indicates the overall reaction in Eq. (I) can be expressed as follows:

$$C_4AF + (MgSO_4)_{aq} \rightarrow \text{Gypsum} + \text{Amorphous (Ca/Fe/Al and Mg phases)} \quad (1)$$

$$\text{Gypsum} + (\text{Ca/Fe/Al phases}) + \text{Residual } C_4AF + (\text{depleting } MgSO_4)_{aq} \rightarrow \text{Gypsum} + \text{AFt} + \text{Amorphous (Ca/Fe and Mg phases)} \quad (2)$$

$$\text{AFt} + \text{Residual } C_4AF + (\text{Ca/Fe/Al phases}) + (\text{depleted } MgSO_4)_{aq} \rightarrow \text{AFm} + \text{Mg/Al Hydroxide Hydrate} + \text{Amorphous (Ca/Fe and Mg phases)} \quad (3)$$

In Eq. (1) calcium from C_4AF is used to form gypsum, while amorphous Ca/Fe/Al and Mg phases are also formed. In Eq. (2) gypsum formation continues, but it is also consumed in the production of AFt; the aluminate consumed in the formation of this phase comes from residual C_4AF and the amorphous Ca/Fe/Al phases. In Eq. (3), AFt converts to AFm, while most of the

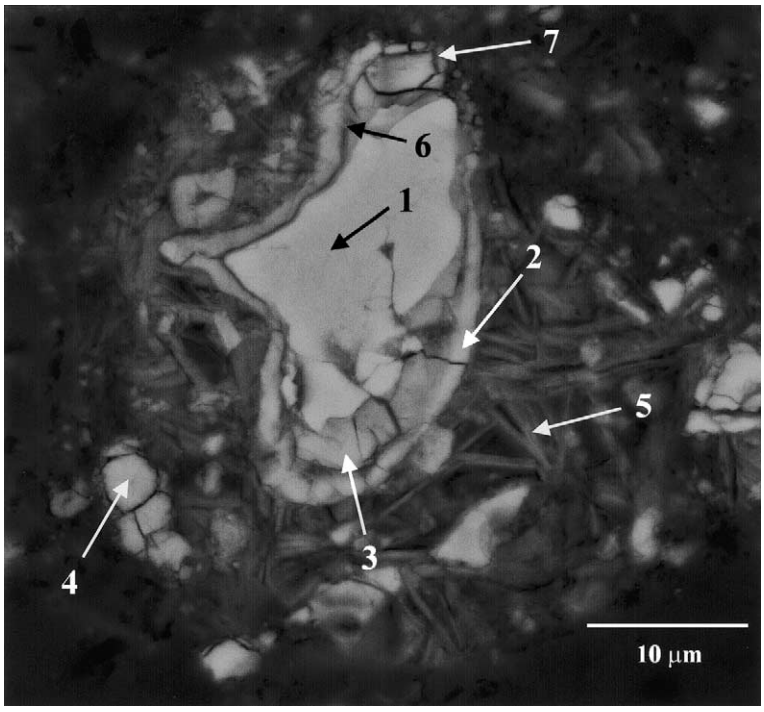

Fig. 10. BSE image of particulate obtained when C_4AF powder is hydrated in 1.0 M $MgSO_4$ solution for 10.6 h.

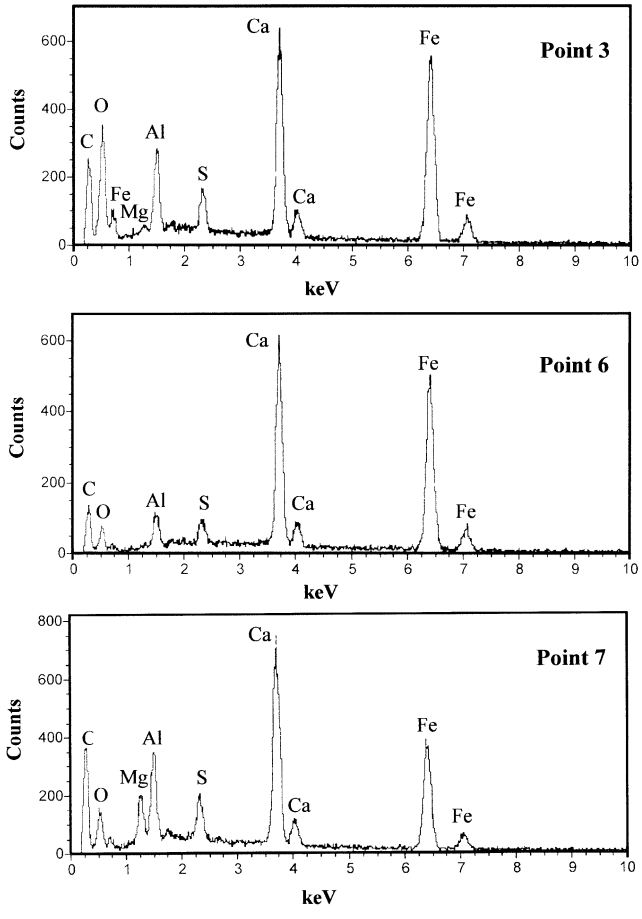

Fig. 11. EDS spectra obtained from points labeled in Fig. 10.

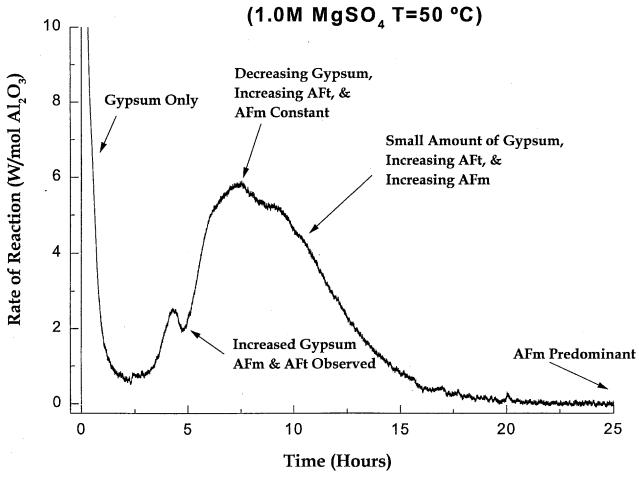

Fig. 12. Rate of heat evolved when C_4AF powder is hydrated in 1.0 M $MgSO_4$ solution, indicating crystalline phases evolved during hydration.

amorphous Mg phases form magnesium aluminate hydroxide hydrate.

5. Conclusions

Hydration of C_4AF in 1.0 $MgSO_4$ solution at a liquid:solids ratio of 3:1 proceeds in three stages: (1) initial gypsum formation, (2) AFm and AFt formation, and (3) AFm and amorphous phase (Mg and Ca/Fe) formation.

Gypsum initially crystallizes as < 5 μm particles, which eventually grow to 30 μm. The gypsum eventually

reacts to form AFt and AFm. Based on this data, AFm forms directly from conversion of ettringite.

Two amorphous phases were observed, Ca/Fe-rich and Mg-rich. Mg-rich phase formation occurs primarily by precipitation from solution, while Ca/Fe-rich phases form in the residual structure of the C_4AF.

Acknowledgements

The authors would like to thank NSF Grant CTS 93-09528 and RJ Lee Group, Inc. for the funding which made this work possible. We would like to also thank Paul Stutzman at NIST for providing the C_4AF.

References

[1] Rasheeduzzafar, Al-Amoudi OSB, Abduljauwad SN, Maslehuddin M. Magnesium–sodium sulfate attack in plain and blended cements. J Mater Civil Eng 1994;6:201–22.

[2] Gollop RS, Taylor HFW. Microstructural and microanalytical studies of sulfate attack – II. Sulfate-resisting portland cement: ferrite composition and hydration chemistry. Cem Concr Res 1994;24(7):1347–58.

[3] Gollop RS, Taylor HFW. Microstructural and microanalytical studies of sulfate attack – III. Sulfate-resisting portland cement: reactions with sodium and magnesium sulfate solutions. Cem Concr Res 1995;25(7):1581–90.

[4] Bonen D, Cohen MD. Magnesium sulfate attack on portland cement paste – I. Microstructural analysis. Cem Concr Res 1992;22:169–80.

[5] Bonen D, Cohen MD. Magnesium sulfate attack on portland cement paste – II. Chemical and mineralogical analyses. Cem Concr Res 1992;22:707–18.

[6] Brown PW, Doerr A. Chemical changes in concrete due to the ingress of aggressive species. Cem Concr Res 2000;30:411–8.

[7] Gollop RS, Taylor HFW. Microstructural and microanalytical studies of sulfate attack – I. Ordinary portland cement paste. Cem Concr Res 1992;22:1027–38.

[8] Taylor HFW. In: Cement chemistry. New York: Academic Press; 1990. p. 396–9.

[9] Taylor HFW. Sulfate reactions in concrete – microstructural and chemical aspects. In: Ceramic transactions.Gartner EM, Uchikawa H, editors. Cem Technol, vol. 40. Westerville, OH: American Ceramic Society; 1994. p. 36–47.

[10] Taylor HFW. In: Cement chemistry. New York: Academic Press; 1990. p. 196–7.

[11] Taylor HFW. In: Cement chemistry. 2nd ed. London: Thomas Telford Services Ltd; 1997. p. 8.

[12] Taylor HFW. In: Cement chemistry. 2nd ed. London: Thomas Telford Services Ltd; 1997. p. 182–5.

[13] Scrivener KL, Pratt PL. Microstructural studies of the hydration of C_3A and C_4AF independently and in cement paste. Br Ceram Proc 1984;35:207–19.

[14] Fukuhara M, Goto S, Asaga K, Daimon M, Kondo R. Mechanisms and kinetics of C_4AF hydration with gypsum. Cem Concr Res 1981;11:407–14.

[15] Brown PW. Early hydration of tetracalcium aluminoferrite in gypsum and lime gypsum solutions. J Am Ceram Soc 1987;70(7):493–6.

[16] Brown PW. Kinetics of tricalcium aluminate and tetracalcium aluminoferrite hydration in the presence of calcium sulfate. J Am Ceram Soc 1993;76(12):2971–6.

[17] Lea FM. In: The chemistry of cement and concrete. Glasgow, Great Britain: Edward Arnold Ltd; 1970. p. 345–55.

[18] Brown PW, Bothe JV. The stability of ettringite. Adv Cem Res 1993;5(18):47–63.

[19] Emanuelson A, Henderson E, Hansen S. Hydration of ferrite Ca_2AlFeO_5 in the presence of sulphates and bases. Cem Concr Res 1996;26(11):1689–94.

[20] Clark BA, Brown PW. Phases formed from hydration of tetracalcium aluminoferrite and magnesium sulfate. Adv Cem Res 1999;11(3):133–7.

[21] Clark A, Brown PW. The formation of monosulfate from tetracalcium aluminoferrite and magnesium sulfate. Adv Cem Res 2000;12(2):71–8.

[22] TenHuisen KS. The formation of biocomposites at physiological temperature. Master of Ceramic Science Thesis, The Pennsylvania State University, College of Earth and Mineral Sciences, 1992.

[23] Brown PW. Phase equilibria and cement hydration. In: Skalny J, editor. Materials science of concrete I. Westerville, OH: American Ceramic Society; 1989. p. 73–94.